

Article

Dominant Aggregate Binding Agent Dynamics of Quaternary Ancient Red Soils under Different Land Use Patterns

Zhongxiu Sun ^{1,2,†}, Siyi Duan ^{2,†}, Yingying Jiang ³, Qiubing Wang ^{2,*} and Ganlin Zhang ^{1,4,5,*}

¹ State Key Laboratory of Soil and Sustainable Agriculture, Institute of Soil Science, Chinese Academy of Sciences, Nanjing 210008, China; zhongxiusun@syau.edu.cn

² College of Land and Environment, Shenyang Agricultural University, Shenyang 110866, China; syduan970127@163.com

³ College of Life Engineering, Shenyang Institute of Technology, Shenyang 113122, China; yingying9111@126.com

⁴ University of Chinese Academy of Sciences, Beijing 100049, China

⁵ Key Laboratory of Watershed Geographic Sciences, Nanjing Institute of Geography and Limnology, Chinese Academy of Sciences, Nanjing 210008, China

* Correspondence: qbwang@syau.edu.cn (Q.W.); glzhang@issas.ac.cn (G.Z.); Tel.: +86-157-3400-5989 (Q.W.); +86-136-0140-5982 (G.Z.)

† These authors contributed equally to this work.

Abstract: The cementation mechanisms and processes of aggregate binding agents are important in understanding aggregate formation. However, the role of threshold values and the proportions of organic and inorganic binding agents in aggregate formation remain unclear. This research investigated the dominant aggregate binding agent dynamics in a sequence comprising buried ancient red soil unaffected by modern climate changes and human activities, alongside nearby exposed Quaternary ancient red soils subjected to different land use patterns influenced by these factors in northeastern China. By analyzing soil age, aggregate compositions, and organic/inorganic indicators of binding agents, including soil organic matter (SOM), free iron oxide (Fed), poorly crystalline iron oxide (Feo), crystalline iron oxide (Fed-Feo), and total clay particles (TCL), we determined the relative contributions of different binding agents using redundancy analysis (RDA). The results revealed that the buried ancient red soil did not contain dominant binding agents in the aggregate formation before 91.01 ka BP. Due to denudation, the buried ancient red soil was exposed at the surface and experienced the importation of soil organic matter, weathering of silicate-bound iron oxides, and crystallization of poorly crystalline iron oxides resulting from the effects of different land use patterns from 91.01 ka to the present. Under the influence of binding agent dynamics, dominant binding agents in the exposed Quaternary ancient red soils' aggregate formation changed into SOM and Fed. When the C/(Fed-Feo) molar ratio was less than 2.13, Fed-Feo was the dominant aggregate binding agent. When the C/(Fed-Feo) molar ratio was greater than 2.13, SOM was the dominant aggregate binding agent. The results of this study improve our understanding of aggregate formation and the relationship between soil organic matter and iron oxides.

Keywords: aggregate composition; organic matter; iron oxides; threshold; aggregate formation



Citation: Sun, Z.; Duan, S.; Jiang, Y.; Wang, Q.; Zhang, G. Dominant Aggregate Binding Agent Dynamics of Quaternary Ancient Red Soils under Different Land Use Patterns. *Agronomy* **2023**, *13*, 1572. <https://doi.org/10.3390/agronomy13061572>

Academic Editor: Zimin Li

Received: 18 May 2023

Revised: 6 June 2023

Accepted: 7 June 2023

Published: 9 June 2023



Copyright: © 2023 by the authors. Licensee MDPI, Basel, Switzerland. This article is an open access article distributed under the terms and conditions of the Creative Commons Attribution (CC BY) license (<https://creativecommons.org/licenses/by/4.0/>).

1. Introduction

Soil aggregates, mostly considered to consist of clay–polyvalent cation–organic matter complexes [1], are secondary particles derived from mineral particles under the cementation effect of binding agents [2]. Their quantity and quality directly affect soil properties and fertility [3]. As basic units of the soil structure, aggregates have the following functions: (a) keeping the soil surface loose; (b) coordinating the water, fertilizer, air, and heat balances in the soil; and (c) maintaining the activity of soil microorganisms and enzymes [4]. The binding agents involved in aggregate formation are mainly divided into organic binding

agents and inorganic binding agents. Organic binding agents can further be divided into transient organic binding agents, such as polysaccharides; temporary organic binding agents, such as roots and fungal mycelia; and persistent organic binding agents, such as polymers with strong adsorption and aromatic compounds with polyvalent cations [5]. By contrast, inorganic binding agents include iron–aluminum oxides and clay particles [6].

The binding mechanism of soil organic matter (SOM) on soil particles is mainly related to the facts that (a) the complex polymers formed by organic molecules can adsorb onto mineral surfaces [7], and (b) amphiphilic organic molecules can be bound around minerals in the form of micelles by different conjugated bonds [8]. Different organic binding agents play different roles in aggregate formation due to their different sources and properties. Polysaccharides participate in aggregate formation as transient organic binding agents due to their easy mineralization [5,9]. They can bind soil particles acting as a type of gelatinous substance [10] or/and a bridge on mineral surfaces [9,11]. Phenols mainly participate in aggregate formation by binding cations to form bonding bridges [12]. Martens [11] reported that the degree of aggregation in a soil with a low phenolic content was lower than in a soil with a higher phenolic content. Lignin is difficult to decompose, making aggregates bound by it more stable than others [13]. Furthermore, mucus produced by microorganisms decomposing lignin can contribute to aggregate formation [14]. Lipids can improve aggregate stability due to their good hydrophobicity [15,16].

In general, iron oxides are present in soils in which aluminum oxides occur, while aluminum oxides are not necessarily present in soils in which iron oxides occur except for red Mediterranean soils, which experienced decalcification, rubefaction, and clay illuviation during pedogenesis and underwent the dissolution and recrystallization of iron and aluminum oxides at the same time [17–21]. Thus, researchers have mostly focused on the effects of iron oxides on aggregate formation and have concluded iron oxides participate in aggregate formation in the following ways: (a) organic molecules can react with iron oxide surfaces [22]; (b) the surfaces of negatively charged clay particles can adsorb positively charged iron oxides via electrostatic action [23]; and (c) iron oxides can act as a bridge between clay surfaces [24]. Different forms of iron oxides have different effects on aggregate formation [21]. Silicate-bound iron oxides as part of the total iron oxides scarcely participate in aggregate formation, while free iron oxides (Fed) as part of the total iron oxides play a role, especially in the aggregation of silt- and clay-sized aggregates to form microaggregates [25]. Moreover, poorly crystalline iron oxides (Feo) in the Fed can provide a large number of hydroxyl groups through the exchange of metal ion ligands with other ligands [26]. When Feo transforms into crystalline iron oxides (Fed-Feo), the relatively small aggregates around them are bound together to form relatively large aggregates [27]. By contrast, clay particles (TCL) mainly participate in aggregate formation through coagulation [28–30]. Sakurai et al. [31] found that negatively charged TCL and positively charged TCL attract each other and cohere under the influence of K^+ and Ca^{2+} plasma. The cohesion level is related to the composition of the clay minerals. For example, TCL containing montmorillonite, which has a larger specific surface area and higher cation exchange capacity, have a stronger effect on cementation [32]. Furthermore, Chen et al. [33] found that TCL can cohere with each other to form microaggregates during dehydration.

Different binding agents worked together in aggregate formation. There were complex relationships of mutual influences and restrictions between different binding agents [34]. In different soils, the dominant binding agent in aggregate formation also differs. Generally, aggregate formation is attributed to the formation and decomposition of organic matter in soils with a relatively high content of organic binding agents and a relatively low content of inorganic binding agents [35,36], such as the typical black soil in northeastern China where the contents of SOM, Fed, and TCL are 69.10, 11.70, and 301.00 g/kg, respectively [27]. However, in soils with a relatively high content of inorganic binding agents and a relatively low content of organic binding agents, aggregate formation is attributed to the transformation of iron oxides in different forms or the coagulation of clay particles [37], such as in the typical red soil in southern China where the contents of SOM, Fed, and TCL are 5.70, 30.40,

and 450.00 g/kg, respectively [27]. However, the threshold value, i.e., the proportions of organic and inorganic binding agents when they play a dominant role in aggregate formation, remains unclear. This inhibits research on the binding mechanism of aggregates.

An evolution sequence consisting of buried and nearby exposed ancient red soils, which is the red paleosol formed in a warm wet climate before the Holocene, in the same stratum under different human activities provides an opportunity to explore aggregate formation. Since this Quaternary ancient red soil has experienced clayification, desilicification, and ferrallitization during pedogenesis, it is rich in a certain amount of inorganic binding agents. Its contents of Fed and TCL range from 17.02 to 23.65 g/kg and 197.00 to 328.90 g/kg, respectively [38]. Moreover, the Quaternary ancient red soil in northern China is mostly buried underground and has a low SOM content (1.57–1.93 g/kg). Parts of the buried ancient red soil have been exposed at the surface via denudation and then affected by different land use patterns, causing the SOM content range to increase to 7.46–30.53 g/kg [39]. The buried ancient red soil was mainly composed of <0.25 mm aggregates, while the exposed Quaternary ancient red soils under different land use patterns were mainly composed of >0.25 mm aggregates [40]. Different aggregate compositions indicate different binding processes during aggregate formation. This leads to the following questions: (a) Was the dominant binding agent different in the aggregate formation of the Quaternary ancient red soil after utilization compared to the buried ancient red soil? (b) If it was different, which binding agent played the dominant role in the aggregate formation of the exposed red soils under different land use patterns? (c) What were the proportions of the organic and inorganic binding agents when organic or inorganic binding agents played a dominant role in the aggregate formation of the red soil? The systematic study of these questions lays a foundation for exploring the aggregate formation of red soils.

2. Materials and Methods

2.1. The Study Area

Based on the Soils of Liaoning [41], the Soil Series of China Liaoning [42], and field investigations, Chaoyang, Liaoning Province, northeastern China, where Quaternary ancient red soils are widely distributed, was selected as the study area (Figure 1a). This region is mountainous and hilly and located in the step boundary zone of the transition from the Inner Mongolia Plateau to the coastal plain. This area has a northern temperate continental monsoon climate, with an annual mean temperature of 5.4–8.7 °C, an annual mean sunshine duration of 2850–2950 h, and an annual mean precipitation of 450–580 mm. The dry period of the area mainly occurs from March to May and September to November, and lasts for approximately 6 months. The main vegetation types are horsetail (*Thymeda triandra*) and elm (*Ulmus propinqua*).

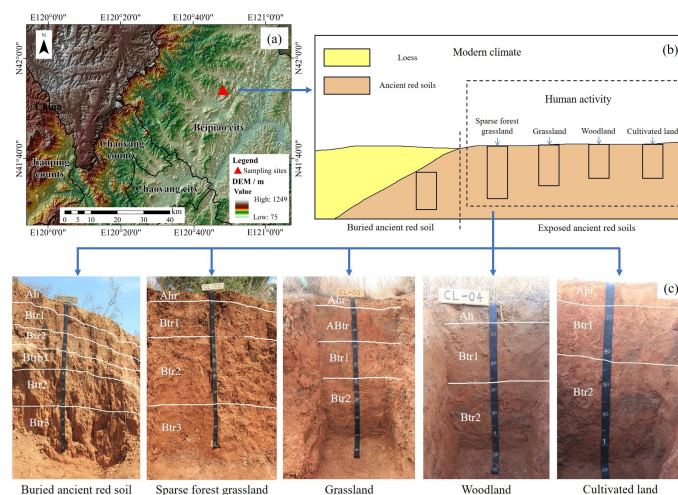


Figure 1. (a) The schematic map showing the location of the study area; (b) The schematic map showing the distribution of the sampling points in the Quaternary ancient red soils. Note: brown color

represents the Quaternary ancient red soil, which is classified as Argosols according to the Chinese Soil Taxonomy [43], Alfisols according to the Soil Taxonomy [44], and Luvisols according to the World Reference Base for Soil Resources [45]; (c) Photos of the Quaternary ancient red soil profiles. Note: “b” indicates that the horizon was buried by other layers; “h” indicates that the horizon has experienced organic matter accumulation processes; “p” indicates that the horizon has been affected by cultivation; “r” indicates that the horizon has experienced oxidation–reduction processes; and “t” indicates that the horizon has experienced clay illuviation processes according to the Manual of Soil Description and Sampling [46].

2.2. Sample Collections and Pretreatments

Quaternary ancient red soil is defined as the red paleosol formed in a warm and wet climate before the Holocene. It is classified as Argosols according to the Chinese Soil Taxonomy [43], Alfisols according to the Soil Taxonomy [44], and Luvisols according to the World Reference Base for Soil Resources [45]. Through several field investigations in the study area, an evolution sequence was found in the stable region of the same Quaternary ancient red soil stratum, where parent material, terrain, biology (before reclamation), climate, and time were uniform (Table 1 and Figure 1b). Quaternary ancient red soils under different land use patterns, influenced by modern climate change and human activities, and the nearby buried Quaternary ancient red soil, scarcely influenced by modern climate change and human activities, were identified. It was impossible to judge whether the wasteland, which might have been affected by land use activities and then abandoned, was undisturbed when collecting ancient red soil samples. There were certain risks if the wasteland was selected as the reference base. At the same time, we attempted to find a reference base such as an ideal wasteland during several field investigations in the study area, but failed. However, a previous study showed that the paleosol (Quaternary ancient red soil) buried more than 50 cm underground was scarcely influenced by external factors, such as modern climate change, human activities, etc. [47], and was closer to the original state of ancient red soil. Therefore, the buried ancient red soil was selected as the reference base in this study. By comparing exposed Quaternary ancient red soils under different land use patterns, influenced by modern climate change and human activities, with the nearby buried ancient red soil in the same stratum, scarcely influenced by modern climate change and human activities, aggregate dominant binding agent dynamics of Quaternary ancient red soils under different land use patterns were explored.

Table 1. Basic information about the sampling points of the Quaternary ancient red soils.

Profile	Parent Material	Altitude (m)	Longitude and Latitude	Land Use Pattern
MC-02	loess	261	41°53'26" N, 120°45'15" E	Buried ancient red soil
CL-02	loess	264	41°53'42" N, 120°45'26" E	Sparse forest grassland
CL-03	loess	269	41°53'40" N, 120°45'30" E	Grassland
CL-04	loess	263	41°53'41" N, 120°45'29" E	Woodland
CL-05	loess	271	41°53'42" N, 120°45'26" E	Cultivated land

For each land use pattern, a typical and representative Quaternary ancient red soil profile was excavated, namely MC-02 (buried ancient red soil with an overlying 0–68 cm thick loess layer), CL-02 (sparse forest grassland where the main vegetation is horsetail and elm), CL-03 (grassland where the main vegetation is horsetail), CL-04 (woodland where the main vegetation is elm), and CL-05 (cultivated land where the main crop is corn) (Table 1 and Figure 1c). According to the Manual of Soil Description and Sampling [46], the genetic horizons and morphological characteristics of the Quaternary ancient red soils under different land use patterns were identified and described (Table 2). Twenty samples from the genetic horizons were collected from the bottom to the surface. Sub-samples of twelve samples from the 0–30 cm surface layer, which were greatly influenced by human

activities, were also collected at 10 cm intervals from the bottom to the surface. Then, the collected samples were transported to the laboratory and naturally air-dried, ground, screened, and set aside for analysis.

Table 2. Profile descriptions of Quaternary ancient red soils.

Profile	Horizon	Depth (m)	Color (Dry)	Texture	Structure	Consistency (Dry)	Others
MC-02	Ah	0–19	2.5YR 5/6	Silty loam	Blocky	Loose	-
	Btr1	19–41	2.5YR 5/8	Silty loam	Prismatic	Moderate hard	Few clay coatings and Fe–Mn nodules
	Btr2	41–68	2.5YR 5/8	Silty loam	Prismatic	Hard	Few clay coatings and Fe–Mn nodules
	Btrb1	68–92	2.5YR 6/6	Silty loam	Prismatic	Hard	Few clay coatings and Fe–Mn nodules
	Btr2	92–141	2.5YR 7/6	Silty loam	Prismatic	Hard	Few clay coatings and Fe–Mn nodules
Btr3	141–210	2.5YR 6/8	Silty loam	Prismatic	Hard	Few clay coatings and Fe–Mn nodules	
CL-02	Ahr	0–17	5YR 6/6	Silty loam	Blocky	Moderately hard	Few clay coatings and Fe–Mn nodules
	Btr1	17–65	5YR 6/8	Silty loam	Prismatic	Hard	Few clay coatings and Fe–Mn nodules
	Btr2	65–151	5YR 6/8	Silty loam	Prismatic	Hard	Few clay coatings and Fe–Mn nodules
	Btr3	151–202	5YR 6/8	Silty clay	Prismatic	Hard	Few clay coatings and Fe–Mn nodules
CL-03	Ahr	0–13	5YR 4/6	Silty loam	Blocky	Moderately hard	Few Fe–Mn nodules
	ABtr	13–51	2.5YR 5/8	Silty clay	Prismatic	Loose	Few clay coatings and Fe–Mn nodules
	Btr1	51–95	5YR 5/8	Silty clay	Prismatic	Medium hard	Few clay coatings and Fe–Mn nodules
	Btr2	95–160	5YR 6/8	Clay loam	Prismatic	Medium hard	Few clay coatings and Fe–Mn nodules
CL-04	Ah	0–16	5YR 4/3	Silty loam	Blocky	Loose	-
	Btr1	16–52	5YR 5/8	Silty loam	Blocky	Moderately hard	Few clay coatings and Fe–Mn nodules
	Btr2	52–120	2.5YR 5/8	Silty clay	Prismatic	Moderately hard	Few clay coatings and Fe–Mn nodules
CL-05	Apr	0–13	5YR 5/8	Silty loam	Blocky	Moderately hard	Few Fe–Mn nodules
	Btr1	13–46	2.5YR 6/6	Silty loam	Blocky	Moderately hard	Few clay coatings and Fe–Mn nodules
	Btr2	46–120	2.5YR 6/8	Silty loam	Blocky	Moderately hard	Few clay coatings and Fe–Mn nodules

Note: “-” indicates that no clay coatings or Fe–Mn nodules were observed.

2.3. Laboratory Methods

Experiments involved in this study were conducted 3 times in parallel with the entire blank test inserted in the measurement process.

2.3.1. Basic Soil Physicochemical Properties

The soil bulk density was determined using the cylindrical core method [48]. For soil age dating, a steel pipe about 30 cm long with one end blocked by caulk was driven into the soil profile and then taken out by removing the surrounding soil with a profile cutter. Then, the steel pipe’s ends were wrapped in tinfoil, and it was transported to the laboratory. Collected samples were further processed according to Wintle [49] and Murray and Wintle [50]. Organics and carbonates in samples were first removed by using H₂O₂ and HCL. Following the first step, sieving and heavy-liquid (Na- or Li-polytungstate) and magnetic separation were conducted to sort quartz sands in samples. HF was finally used to etch the outermost “rind” on quartz. The optically stimulated luminescence signal strength was determined by a Daybreak 1100 A (Daybreak Company, South Jordan, UT, USA). For the soil pH, 10.00 g soil was sieved through a 10-mesh nylon sieve and placed in a small beaker. Then, 25 mL distilled water with CO₂ removed was added. After being stirred for 1 min and left to stand for 30 min, the sample was measured using a pH meter (PHSJ-3F, Shanghai, China). For the elemental analysis of Ti and Zr, 10.00 g soil was passed through a 300-mesh nylon sieve and placed in a small box. Then, a portable X-ray fluorescence instrument (PANalytical 2004, PANalytical Company, Almelo, The Netherlands) was used to scan the sample’s center for 90 s to determine the contents of Ti and Zr.

2.3.2. Soil Aggregates

According to soil aggregate stability, aggregates are mainly divided into mechanically stable aggregates and water-stable aggregates, which were obtained using the dry-sieving and wet-sieving methods, respectively [51,52]. Since the Quaternary ancient red soil was sticky and heavy, it became very hard after air-drying, and it was difficult to accurately separate the mechanically stable aggregates into different size fractions. Moreover, the dry-

sieving method was greatly affected by human factors, resulting in poor repeatability and an inaccurate data distribution [52,53]. Therefore, the wet-sieving method [54] was selected in this study to separate the water-stable aggregates of the investigated Quaternary ancient red soils. To systematically explore the dominant aggregate binding agent dynamics of the Quaternary ancient red soils under different land use patterns, a relatively fine grading method of aggregate size fractions was adopted [40], and the specific steps were as follows: A set of sieves with mesh sizes of 5, 2, 1, 0.5, 0.25, and <0.053 mm were placed in the tank of the aggregate structure analyzer (XY-100, Dingsheng Ronghe Technology Co., LTD., Qingdao, China). Then, 50.00 g soil was placed in the 5 mm sieve and submerged for 3 min. The sample was shaken for 10 min with 30 rounds per minute and then taken out and placed in a drying container. After discarding the supernatant and drying and weighing the sample, the aggregate weight of each size fraction was obtained. The proportions of aggregates of different size fractions were calculated as follows [55] (except the proportion of the <0.053 mm aggregate, which was calculated using difference subtraction):

$$W_i = \frac{w_i}{m} \times 100\% \quad (1)$$

where i is the aggregate size fraction, w_i is the mass of aggregates in size fraction i , W_i is the proportion of aggregates in size fraction i , and m is the total mass of the sample.

2.3.3. Soil Aggregate Binding Agents

Soil Organic Matter

Following the analytical procedure described by Li et al. [56], the 40–50 mg 100-mesh sample was placed in a tin boat. After being packed and compacted, the sample was measured using an element analyzer (Vario EL III, Elementar Company, Langensfeld, Germany) to obtain the content of soil organic carbon (SOC). The content of SOM was calculated as follows:

$$SOM = SOC \times 1.724 \quad (2)$$

where SOM is the soil organic matter content, SOC is the soil organic carbon content, and 1.724 is the conversion coefficient of soil organic carbon to soil organic matter.

Soil Free Iron Oxide

Following the method proposed by Mehra and Jackson [57], the 1.00 g 60-mesh soil was placed in a centrifuge tube. Then, 20 mL 0.2 mol/L sodium citrate and 2.5 mL 1 mol/L NaHCO₃ were added. After being heated to 80 ± 5 °C in a thermostatic water bath oscillator (SHZ-82, Qingdao, China), the sample was added into 0.5 g sodium hydrosulfite and shaken for 15 min. After cooling, the sample was centrifuged for 40 min with 3500 rounds per minute in a centrifugal machine (L530, Xiangyi Centrifuge Co., Ltd., Changsha, China). After being transferred to a 100 mL volumetric bottle, the supernatant was diluted 10 times with distilled water. The sediment in the centrifuge tube then underwent the above process twice more. An atomic absorption spectrophotometer (Z-2000, HITACHI, Tokyo, Japan) was used to measure the content of Fe. Formula (3) was used to convert the Fe content of the supernatant into that of the sample.

$$Fe_2O_3 = \frac{C \times V \times 10 \times 1.43}{m} \quad (3)$$

where Fe_2O_3 is the free iron oxide content of the sample, C is the free iron oxide content of the supernatant, V is the constant volume, 10 is the dilution ration, 1.43 is the conversion coefficient of Fe to Fe_2O_3 , and m is the total mass of the sample.

Soil Poorly Crystalline Iron Oxide

Following the method proposed by McKeague and Day [58], the 1.00 g 60-mesh soil was placed in conical flasks. Then, 50 mL 0.2 mol/L ammonium oxalate acid was added.

After being shaken for 2 h under shade, the sample was filtered, diluted fivefold and then measured by an atomic absorption spectrophotometer (Z-2000, HITACHI, Tokyo, Japan) to obtain the content of Feo. Formula (4) was used to convert the Feo content of the supernatant into that of the sample.

$$\text{Fe}_2\text{O}_3 = \frac{C \times V \times 5 \times 1.43}{m} \quad (4)$$

where Fe_2O_3 is the poorly crystalline iron oxide content of the sample, C is the poorly crystalline iron oxide content of the supernatant, V is the constant volume, 5 is the dilution ratio, 1.43 is the conversion coefficient of Fe to Fe_2O_3 , and m is the total mass of the sample.

Soil Crystalline Iron Oxide

The content of soil crystalline iron oxide (Fed-Feo) was calculated by difference subtraction between the content of free iron oxide and the content of poorly crystalline iron oxide.

Soil Total Clay Particle

Following the analytical procedure described by Lu and An [59], the 0.50 g 10-mesh soil was placed in a small beaker. Then, 15 mL 10% H_2O_2 was added. After standing for 24 h, the sample was heated to remove excess H_2O_2 and added into 1 mL 0.5 mol/L NaOH while cooling. After standing for another 24 h, the sample was ultrasonically shaken for 10 min and then analyzed with a laser diffraction particle analyzer (Mastersizer 3000, Marvin Instruments Ltd., Marvin, UK) to determine the particle size distribution. The content of TCL was defined by the percentage of $<2 \mu\text{m}$ particles for all size fractions in the sample.

2.4. Redundancy Analysis

Redundancy analysis (RDA), an ordination method, is commonly used to explain the relationship between explanatory factors and response variables in ecological studies. It can comprehensively analyze the influence of multiple variables and is often used to effectively evaluate the influence of one set of variables on others. In the results of redundancy analysis, the axis represents the ordination of fitting values of the linear model, and the eigenvalue represents the weight of the axis. The relative contribution rate of the axis is calculated by the proportion of the eigenvalue of the axis to the total eigenvalue of all axes. However, not every axis is reasonable and effective, but the significance of each axis should be tested using Monte Carlo permutation. The results are reliable only when the Monte Carlo permutation on all axes is significant, meaning the result can explain the relationship between explanatory factors and response variables. In the ordination diagram of redundancy analysis, scatter points represent samples, and arrows represent explanatory factors and response variables. The included angle between variable arrows represents the correlation between variables. If the included angle is less than 90° , it indicates that there is a positive correlation between variables. If the included angle is greater than 90° , it indicates a negative correlation between variables. Generally, results of redundancy analysis represent the relative relationship or contribution between variables instead of the absolute relationship or contribution between variables.

2.5. Data Processing and Analysis

SPSS 23.0 and Canoco 5.0 were used to statistically analyze data, and Sigmaplot 12.5 was used to draw diagrams.

3. Results

3.1. Determining the Uniformity of the Parent Material

Analysis of the field morphology is the most direct and intuitive way to determine the uniformity of the parent material [60]. As shown in Table 2, horizons Btrb1, Btr2, and Btr3 of the buried ancient red soil had a silty loam texture, few Fe–Mn nodules and clay

coatings, a blocky structure, 2.5YR hue values ranging from 6 to 7, chroma values ranging from 6 to 8, and a hard consistency under dry conditions (Table 2). This indicates that the buried ancient red soil had uniform morphological characteristics, and the characteristics were well preserved before utilization. As it had been exposed at the surface through denudation, the Quaternary ancient red soil was affected by human activities, and its structure and consistency did not change, while its color and texture changed (Table 2). Compared with the buried ancient red soil, the texture of certain topsoil or subsoil of the exposed ancient red soils after utilization changed from silty loam to silty clay or clay loam, while the hue increased to 5YR and the hue value decreased to a range of 4–6. However, these morphological differences should be attributed to pedogenesis and the uniformity of the parent material could not be directly determined. More indexes need to be combined to determine the uniformity of the parent material of the investigated Quaternary ancient red soils.

Previous studies have shown that the clay-free particle size distribution and Ti/Zr ratio are acceptable indexes for determining the uniformity of the parent material [60,61]. As shown in Figure 2, these indexes were distributed uniformly with depth. Their variation coefficients ranged from 1.43% to 15.12% within the investigated Quaternary ancient red soil profiles and from 3.75% to 9.90% between the investigated Quaternary ancient red soil profiles (Table 3). The variation coefficients of all the indexes within and between the investigated Quaternary ancient red soils were below the standard indicating that the parent material is uniform, i.e., if the variation coefficient of the determining indicator is less than 22% [62]. In addition, previous research found the red soil in the study area was mainly composed of illite, smectite, and kaolinite and distributed uniformly with depth [63,64]. This indicated the sequence had a uniform parent material.

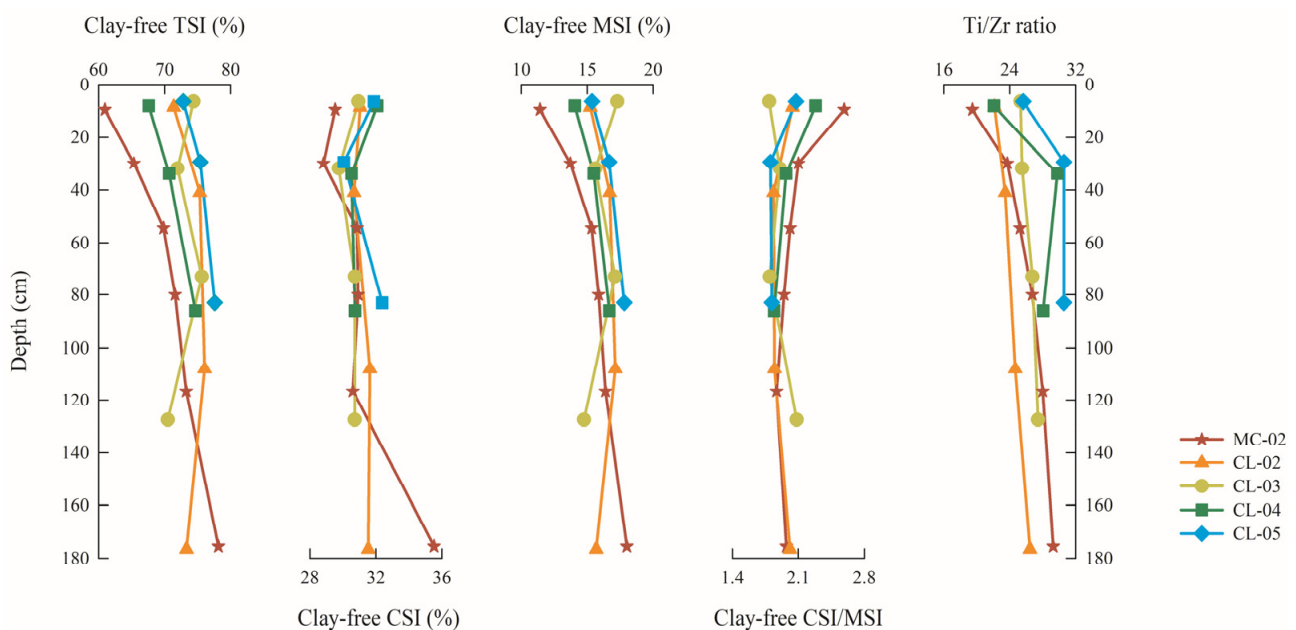


Figure 2. Distributions of the clay-free TSI, CSI, MSI, CSI/MSI, and Ti/Zr values of the Quaternary ancient red soils with depth under different land use patterns. Note: MC-02 represents the buried ancient red soil; CL-02 represents the sparse forest grassland; CL-03 represents the grassland; CL-04 represents the woodland; CL-05 represents the cultivated land; TSI represents the total silt; CSI represents the coarse silt; MSI represents the medium silt.

Table 3. Variation coefficients of clay-free TSI, CSI, MSI, CSI/MSI, and Ti/Zr of the Quaternary ancient red soils under different land use patterns.

Profile	Clay-Free TSI (%)			Clay-Free CSI (%)			Clay-Free MSI (%)			Clay-Free CSI/MSI			Ti/Zr Ratio		
	Mean	S.D.	C.V.	Mean	S.D.	C.V.	Mean	S.D.	C.V.	Mean	S.D.	CV.	Mean	S.D.	C.V.
MC-02	74.32	3.41	4.58%	32.34	2.75	8.51%	16.74	1.11	6.66%	1.93	0.05	2.83%	28.01	1.27	4.52%
CL-02	74.00	2.11	2.85%	31.22	0.45	1.43%	16.18	0.88	5.41%	1.93	0.11	5.47%	24.19	1.83	7.57%
CL-03	73.10	2.32	3.18%	30.53	0.53	1.74%	16.19	1.21	7.48%	1.89	0.14	7.19%	26.25	1.01	3.86%
CL-04	70.97	3.53	4.98%	31.10	0.84	2.71%	15.40	1.31	8.53%	2.03	0.23	11.14%	26.65	4.03	15.12%
CL-05	75.27	2.39	3.18%	31.43	1.23	3.90%	16.60	1.22	7.35%	1.90	0.15	8.02%	28.93	2.85	9.84%
Total	73.53	2.76	3.75%	31.27	1.29	4.14%	16.22	1.09	6.70%	1.93	0.13	6.87%	26.62	2.63	9.90%

Note: S.D. denotes standard deviation; C.V. denotes coefficient of variation.

3.2. Aggregate Composition

On the premise of determining the uniformity of the parent material of the investigated Quaternary ancient red soils, horizon Btr2 of the buried ancient red soil, which exhibited the weakest weathering and the least development, was selected as the reference basis [65] and its age was dated (Figure 3). The aggregate compositions of 0–10, 10–20, and 20–30 cm horizons of the exposed Quaternary ancient red soils under different land use patterns and horizon Btr2 of the buried ancient red soil were determined (Figure 3).

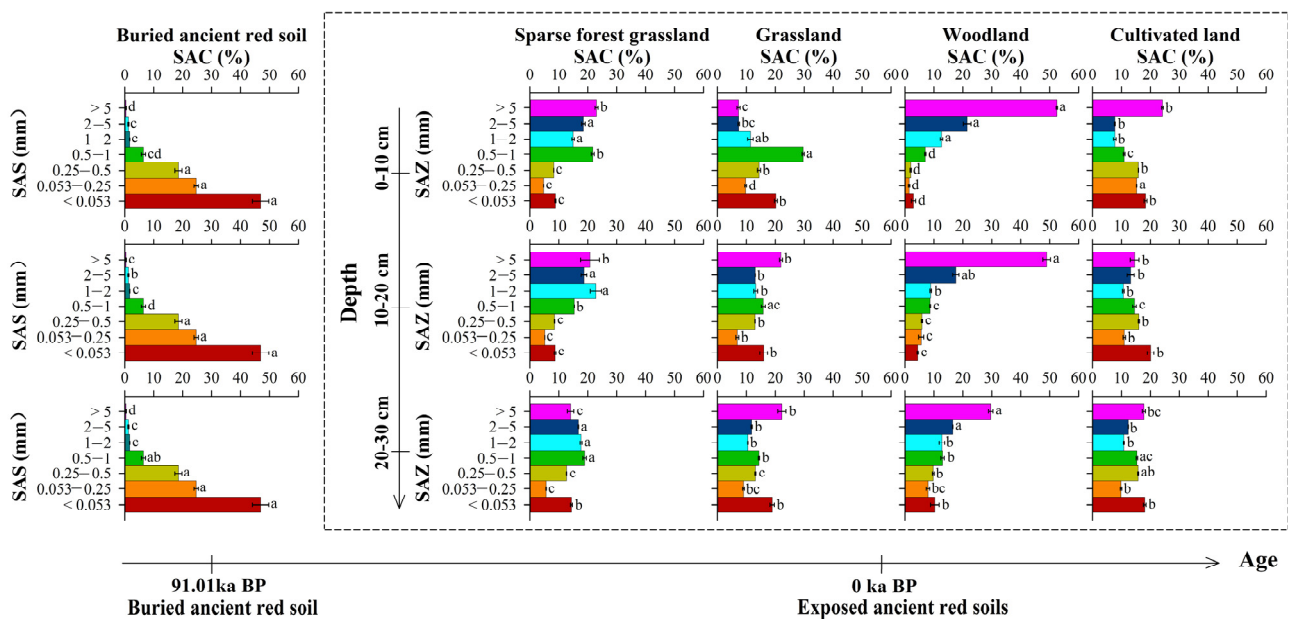


Figure 3. Aggregate compositions of the 0–30 cm depth horizon of the Quaternary ancient red soils under different land use patterns. Note: the different lowercase letters indicate significant differences in the aggregate contents of the same size within the same depth for the Quaternary ancient red soils under different land use patterns ($p < 0.05$); SAZ represents the soil aggregate size; SAC represents the soil aggregate content.

Before 91.01 ka BP, the buried ancient red soil was mainly composed of <0.25 mm aggregates, comprising 71.62% of the total aggregates. The <0.053 mm aggregate content was the highest, accounting for 48.84%. From 91.01 ka to the present, the Quaternary ancient red soil was exposed at the surface through denudation and was then affected by human activities. Compared with the buried ancient red soil, the contents of the >5, 2–5, 1–2, and 0.5–1 mm aggregates within the 0–30 cm depth region of the exposed Quaternary ancient red soils were greater after utilization, while the contents of the 0.25–0.5, 0.053–0.25, and <0.053 mm aggregates were lower. This led to a change in the aggregate composition from mainly <0.25 mm aggregates to mainly >0.25 mm aggregates. The average >0.25 mm

aggregate content of the 0–30 cm depth horizon was the highest in the woodland, followed by the sparse forest grassland and the grassland, and the lowest in the cultivated land. Although the aggregate composition of the 0–30 cm depth horizon of the exposed ancient red soils after utilization exhibited a similar trend, there were differences in the aggregate compositions between them due to influences of different land use activities. Among them, the average > 5 mm aggregate content of the 0–30 cm depth horizon in the sparse forest grassland was the highest, accounting for 19.29%. The average 0.5–1 mm aggregate content of the 0–30 cm depth horizon in the grassland was the highest, accounting for 19.94%. The average > 5 mm aggregate content of the 0–30 cm depth horizon in the woodland was the highest, accounting for 43.70%. The average > 5 mm aggregate content of the 0–30 cm depth horizon in the cultivated land was the highest, accounting for 18.84% (Figure 3).

3.3. Aggregate Binding Agent Composition

This evolution sequence of Quaternary ancient red soil had a pH value ranging from 5.58 to 6.10, which did not indicate the presence of calcium carbonate. Furthermore, no observable CaCO₃, such as pseudomycelium and calcareous concretions, was detected in red soil profiles as verified by the lime reaction test and lab data, demonstrating that profiles had already undergone intense leaching for clay and Fe–Mn eluviation and illuviation. Thus, SOM, Fed, Feo, Fed-Feo, and TCL contents were selected as indicators of the binding agents and were used to explore the aggregate binding agent compositions of the investigated Quaternary ancient red soils (Figure 4).

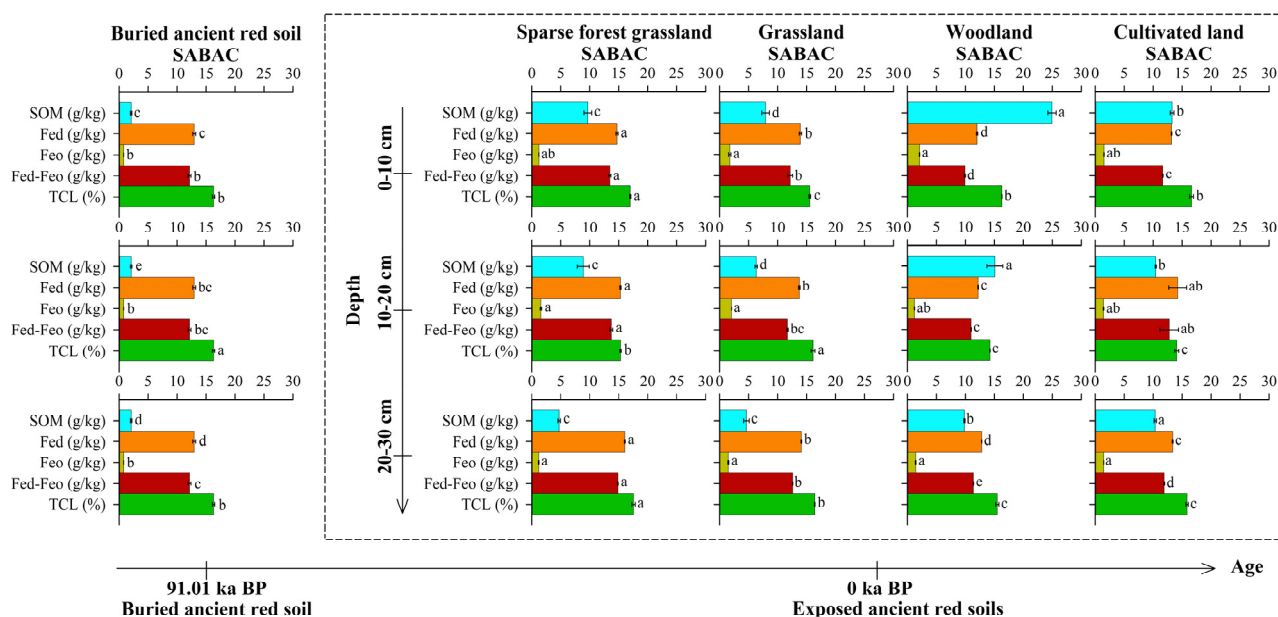


Figure 4. Aggregate binding agent compositions of the 0–30 cm depth horizon of the Quaternary ancient red soils under different land use patterns. Note: The different lowercase letters indicate significant differences in the same aggregate binding agent at the same depth for the Quaternary ancient red soils under different land use patterns ($p < 0.05$); SABAC represents the soil aggregate binding agent content.

3.3.1. Soil Organic Matter

Before 91.01 ka BP, the Quaternary ancient red soil was buried under loess and had a low SOM content (2.08 g/kg). From 91.01 ka to the present, the Quaternary ancient red soil was exposed at the surface through denudation and then affected by different human activities. Compared with the buried ancient red soil, the SOM content of the 0–30 cm depth horizon of the exposed ancient red soils under different land use patterns was significantly higher. The SOM content of the 0–10 cm depth horizon was the highest in the woodland, followed by the cultivated land and the sparse forest grassland, and it was the lowest in the

grassland, with values of 24.95, 13.27, 9.67, and 7.94 g/kg, respectively. The SOM content of the 10–20 cm depth horizon was the highest in the woodland, followed by the cultivated land and the sparse forest grassland, and it was the lowest in the grassland, with values of 15.10, 10.45, 8.88, and 6.32 g/kg, respectively. The SOM content of the 20–30 cm depth horizon was the highest in the cultivated land, followed by the woodland and the sparse forest grassland, and it was the lowest in the grassland, with values of 10.36, 9.84, 4.72, and 4.63 g/kg, respectively (Figure 4).

3.3.2. Iron Oxides in Different Forms

Free Iron Oxide

Before 91.01 ka BP, the Quaternary ancient red soil was buried under loess with a Fed content of 12.94 g/kg. From 91.01 ka to the present, the Quaternary ancient red soil was exposed at the surface through denudation and then affected by different human activities. Compared with the buried ancient red soil, the Fed content of the 0–30 cm depth horizon of the sparse forest grassland, grassland, and cultivated land was higher, while that of the woodland was lower. The Fed content of the 0–10 cm depth horizon was the highest in the sparse forest grassland, followed by the grassland and the cultivated land, and it was the lowest in the woodland, with values of 14.71, 13.94, 13.17, and 12.02 g/kg, respectively. The Fed content of the 10–20 cm depth horizon was the highest in the sparse forest grassland, followed by the cultivated land and the grassland, and it was the lowest in the woodland, with values of 15.30, 14.22, 13.76, and 12.21 g/kg, respectively. The Fed content of the 20–30 cm depth horizon was the highest in the sparse forest grassland, followed by the grassland and the cultivated land, and it was the lowest in the woodland, with values of 16.05, 14.10, 13.37, and 12.82 g/kg, respectively (Figure 4).

Poorly Crystalline Iron Oxide

Before 91.01 ka BP, the Quaternary ancient red soil was buried under loess and had a low Feo content (0.79 g/kg). From 91.01 ka to the present, the Quaternary ancient red soil was exposed at the surface through denudation and then affected by different human activities. Compared with the buried ancient red soil, the Feo contents of the 0–30 cm depth horizon of the exposed ancient red soils under different land use patterns were higher. The Feo content of the 0–10 cm depth horizon was the highest in the woodland, followed by the grassland and the cultivated land, and it was the lowest in the sparse forest grassland, with values of 2.10, 1.75, 1.52, and 1.23 g/kg, respectively. The Feo content of the 10–20 cm depth horizon was the highest in the grassland, followed by the sparse forest grassland and the cultivated land, and it was the lowest in the woodland, with values of 2.04, 1.57, 1.44, and 1.22 g/kg, respectively. The Feo content of the 20–30 cm depth horizon was the highest in the grassland, followed by the cultivated land and the woodland, and it was the lowest in the sparse forest grassland, with values of 1.50, 1.48, 1.43, and 1.19 g/kg, respectively (Figure 4).

Crystalline Iron Oxide

Before 91.01 ka BP, the Quaternary ancient red soil was buried under loess with a Fed-Feo content of 12.15 g/kg. From 91.01 ka to the present, the Quaternary ancient red soil was exposed at the surface through denudation and then affected by human activities. When compared with the buried ancient red soil, the Fed-Feo content of the 0–30 cm depth horizon of the exposed ancient red soils under different land use patterns did not reveal similar trends. The Fed-Feo contents of the 0–10 cm depth horizon in the sparse forest grassland and grassland were higher, while those of the woodland and the cultivated land were lower. The Fed-Feo content of the 0–10 cm depth horizon was the highest in the sparse forest grassland, followed by the grassland and the cultivated land, and it was the lowest in the woodland, with values of 13.47, 12.19, 11.65, and 9.92 g/kg, respectively. The Fed-Feo contents of the 10–20 cm depth horizon of the sparse forest grassland and the cultivated land were higher, while those of the grassland and the woodland were lower. The Fed-Feo

content of the 10–20 cm depth horizon was the highest in the sparse forest grassland, followed by the cultivated land and the grassland, and it was the lowest in the woodland, with values of 13.73, 12.78, 11.72, and 10.99 g/kg, respectively. The Fed-Feo contents of the 20–30 cm depth horizon of the sparse forest grassland and the grassland were higher, while those of the cultivated land and the woodland were lower. The Fed-Feo content of the 20–30 cm depth horizon was the highest in the sparse forest grassland, followed by the grassland and the cultivated land, and it was the lowest in the woodland, with values of 14.86, 12.60, 11.89, and 11.39 g/kg, respectively (Figure 4).

3.3.3. Clay Particles

Before 91.01 ka BP, the Quaternary ancient red soil was buried under loess with a TCL content of 16.29%. From 91.01 ka to the present, the Quaternary ancient red soil was exposed at the surface through denudation and then affected by human activities. When compared with the buried ancient red soil, the TCL content of the 0–30 cm depth horizon of the exposed ancient red soils under different land use patterns did not reveal similar trends. The TCL contents of the 0–10 cm depth horizon of the sparse forest grassland, the woodland, and the cultivated land were higher, while that of the grassland was lower. The TCL content of the 0–10 cm depth horizon was the highest in the sparse forest grassland, followed by the cultivated land and the woodland, and it was the lowest in the grassland, with values of 16.99%, 16.62%, 16.31%, and 15.55%, respectively. The TCL contents of the 10–20 cm horizon of the exposed ancient red soils under different land use patterns were lower. It was the highest in the grassland, followed by the sparse forest grassland and the woodland, and it was the lowest in the cultivated land, with values of 16.12%, 15.31%, 14.25%, and 14.07%, respectively. The TCL content of the 20–30 cm depth horizon of the exposed ancient red soils under different land use patterns was higher. It was the highest in the sparse forest grassland, followed by the grassland and the cultivated land, and it was the lowest in the woodland, with values of 17.55%, 16.42%, 15.84%, and 15.50%, respectively (Figure 4).

3.4. Determining the Dominant Aggregate Binding Agent of the Investigated Quaternary Ancient Red Soils

To determine the dominant aggregate binding agent of the investigated Quaternary ancient red soils, RDA was carried out by selecting the buried ancient red soil, the sparse forest grassland, the grassland, and the cultivated land as samples, selecting the SOM, Fed, and TCL contents as the explanatory factors, and selecting the >5, 2–5, 1–2, 0.5–1, 0.25–0.5, 0.053–0.25, and <0.053 mm aggregate contents as the response variables (Figure 5a). The cumulative explained percentage of the first three RDA axes accounted for 100%. The Monte Carlo permutation test on all of the RDA axes reached a significant level ($p < 0.05$), indicating the RDA results are reliable and can explain the relationship between the aggregate compositions and aggregate binding agents of the investigated Quaternary ancient red soils. The relative contribution rate of the aggregate binding agents was the highest for SOM, followed by Fed, and that of TCL was the lowest, with values of 72.00%, 26.40%, and 1.50%, respectively (Figure 5d). Among them, SOM and Fed had significant effects on aggregate compositions ($p < 0.05$), while TCL did not ($p > 0.05$). This indicated that SOM and Fed were the dominant aggregate binding agents of the investigated Quaternary ancient red soils, while the effect of TCL was not obvious.

However, the aggregate composition of the Quaternary ancient red soils after utilization changed greatly (Figure 3), indicating that the aggregate binding process had changed. To further explore the dominant aggregate binding agent dynamics of the Quaternary ancient red soils under different land use patterns, RDA was carried out separately for the buried ancient red soil and the exposed Quaternary ancient red soils after utilization.

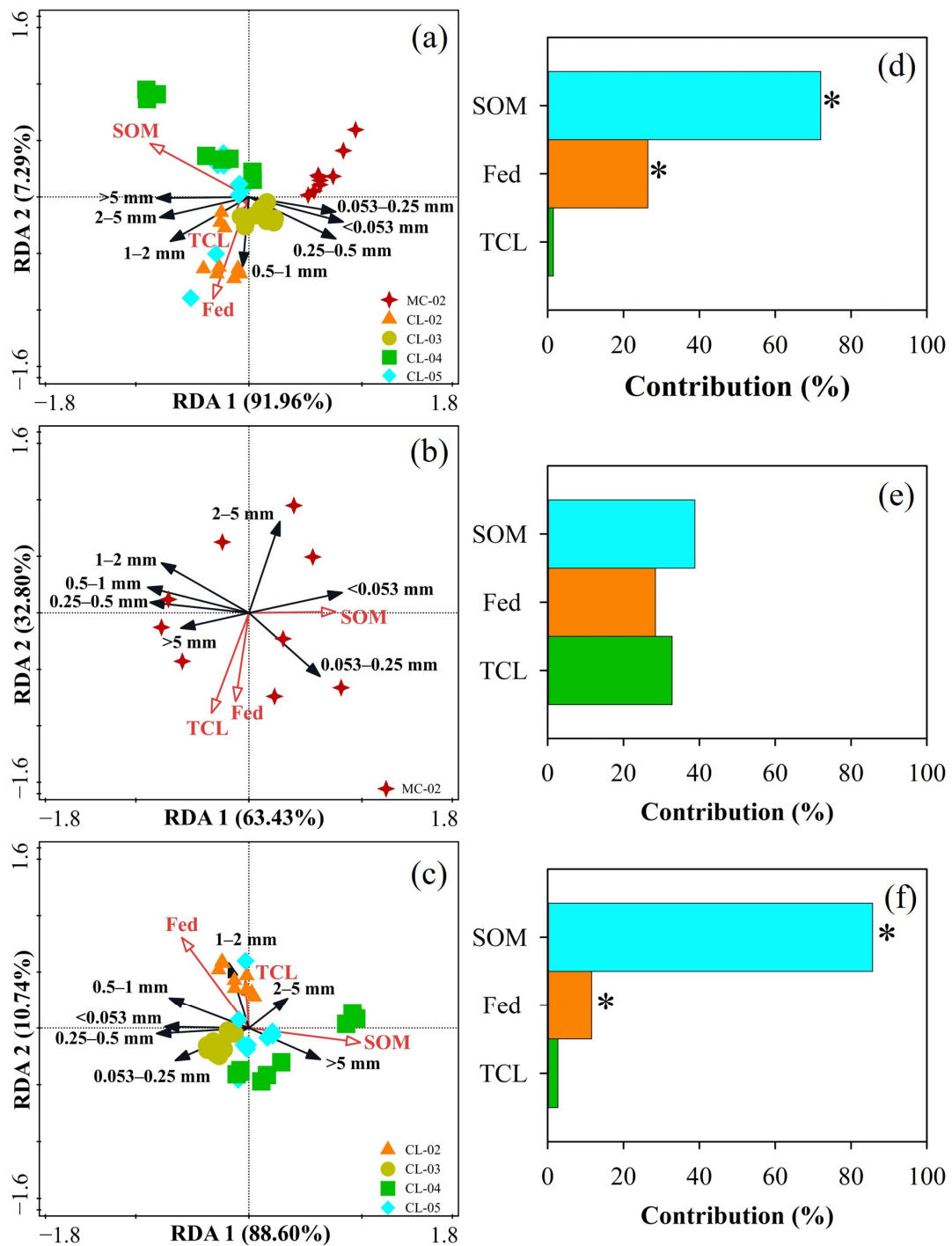


Figure 5. Ordination diagram of the redundancy analysis of the relationship between the aggregate compositions and aggregate binding agents of (a) the investigated Quaternary ancient red soils, (b) the buried ancient red soils, and (c) the exposed Quaternary ancient red soils after utilization; and the relative contribution rates of the redundancy analysis of the relationship between the aggregate compositions and aggregate binding agents of (d) the investigated Quaternary ancient red soils, (e) the buried ancient red soils, and (f) the exposed Quaternary ancient red soils after utilization. SOM—soil organic matter; Fed—free iron oxide; and TCL—total clay particles. “*” indicates that the binding agent has a significant effect on the aggregate compositions ($p < 0.05$).

3.4.1. Buried Ancient Red Soil

RDA was carried out by selecting the buried ancient red soil as the sample, selecting the SOM, Fed, and TCL contents as the explanatory factors, and selecting the >5, 2–5, 1–2, 0.5–1, 0.25–0.5, 0.053–0.25, and <0.053 mm aggregate contents as the response variables (Figure 5b). The cumulative explained percentage of the first three RDA axes accounted for 100%. However, the Monte Carlo permutation test conducted on all of the RDA axes did not reach a significant level ($p > 0.05$). This indicated the RDA results are not reliable and cannot explain the relationship between the aggregate compositions and aggregate binding agents. SOM, Fed, and TCL played a certain role in the aggregate formation of the buried ancient red soil, but they were not the dominant binding agents.

3.4.2. Exposed Quaternary Ancient Red Soils under Different Land Use Patterns

RDA was carried out by selecting the sparse forest grassland, the grassland, the woodland, and the cultivated land as the samples, selecting the SOM, Fed, and TCL contents as the explanatory factors, and selecting the >5, 2–5, 1–2, 0.5–1, 0.25–0.5, 0.053–0.25, and <0.053 mm aggregate contents as the response variables (Figure 5c). The cumulative explained percentage of the first three RDA axes was 100%. The Monte Carlo permutation test conducted on all of the RDA axes reached a significant level ($p < 0.05$), indicating the RDA results are reliable and can explain the relationship between aggregate compositions and aggregate binding agents. The relative contribution rate of the aggregate binding agents was the highest for SOM, followed by Fed, and was the lowest for TCL, with values of 85.70%, 11.60%, and 2.70%, respectively (Figure 5f). Among them, SOM and Fed had significant effects on aggregate compositions ($p < 0.05$), while TCL did not ($p > 0.05$), indicating that SOM and Fed were the dominant aggregate binding agents of the exposed ancient red soils after utilization, while the effect of TCL was not obvious.

Since there were still differences between the aggregate compositions of the exposed Quaternary ancient red soils under different land use patterns (Figure 3), RDA was carried out separately by selecting the sparse forest grassland, the grassland, the woodland, and the cultivated land as the samples, selecting the SOM, Feo, and Fed-Feo contents as the explanatory factors, and selecting the >5, 2–5, 1–2, 0.5–1, 0.25–0.5, 0.053–0.25, and <0.053 mm aggregates contents as the response variables (Figure 6). The Monte Carlo permutation test conducted on all of the RDA axes of the sparse forest grassland, the woodland, and the cultivated land reached a significant level ($p < 0.05$), indicating the RDA results are reliable and can explain the relationship between aggregate compositions and aggregate binding agents (Figure 6a,c,d). However, that of the grassland did not reach a significant level ($p < 0.05$), indicating the RDA results are not reliable and cannot explain the relationship between aggregate compositions and aggregate binding agents (Figure 6b). SOM, Feo, and Fed-Feo played a certain role in the aggregate formation of the grassland, but they were not the dominant binding agents. Based on the Monte Carlo permutation test on the aggregate binding agents, Fed-Feo was the dominant aggregate binding agent of the sparse forest grassland, with a relative contribution rate of 74.20% (Figure 6e), while SOM was the dominant aggregate binding agent of the woodland and the cultivated land, with relative contribution rates of 90.50% and 86.10%, respectively (Figure 6g,h).

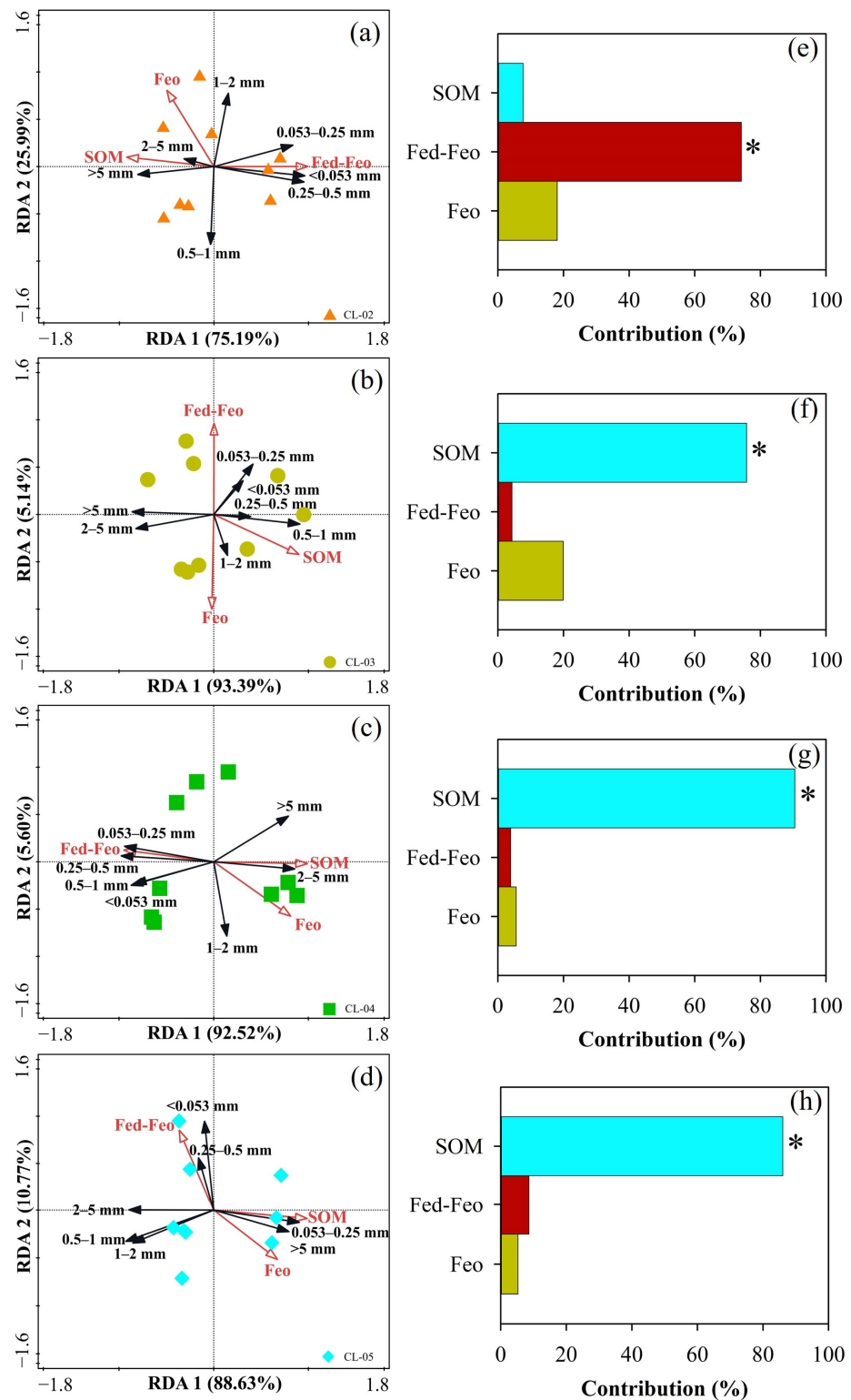


Figure 6. Ordination diagram of the redundancy analysis of the relationship between the aggregate compositions and aggregate binding agents of (a) the sparse forest grassland, (b) the grassland, (c) the woodland, and (d) the cultivated land; and the relative contribution rates of the redundancy analysis on the relationship between the aggregate compositions and aggregate binding agents of (e) the sparse forest grassland, (f) the grassland, (g) the woodland, and (h) the cultivated land. SOM—soil organic matter; Fed-Feo—crystalline iron oxide; and Feo—poorly crystalline iron oxide. “*” indicates that the aggregate binding agent has a significant effect on the aggregate compositions ($p < 0.05$).

4. Discussion

4.1. Soil Organic Matter and Iron Oxide Dynamics of the Quaternary Ancient Red Soils under Different Land Use Patterns

To obtain reliable Quaternary red soil dynamics information, the first step is to determine its parent material uniformity. This is mainly because the soil property changes of the sequence can be attributed to pedogenesis only when the parent material of the investigated Quaternary ancient soil is uniform [65,66]. The investigated Quaternary ancient red soil had a silty loam, silty clay, or clay loam texture, few Fe–Mn nodules and clay coatings, a blocky structure, hues ranging from 2.5YR to 5YR, and a hard consistency under dry conditions (Table 2). This indicated that the evolution sequence of Quaternary ancient red soil had uniform morphological characteristics. In addition, the variation coefficients of the clay-free particle size distribution and Ti/Zr ratio within and between the investigated Quaternary ancient red soils were all below the standard (22%) [62]. What is more, researchers found the red soil in the study area was mainly composed of illite, smectite, and kaolinite and distributed uniformly with depth [63,64]. Above all, the evolution sequence provided reliable research materials for exploring the dominant aggregate binding agent dynamics of Quaternary ancient red soils under different land use patterns.

Before 91.01 ka BP, the Quaternary ancient red soil was buried under loess and had a low SOM content (2.08 g/kg), due to few disturbances and almost no importation of foreign organic matter. From 91.01 ka to the present, the Quaternary ancient red soil was exposed at the surface through denudation and then affected by different human activities. Compared with the buried ancient red soil, the SOM contents of the 0–30 cm depth horizon of the exposed ancient red soils under different land use patterns were higher due to vegetation return and fertilization [39]. Since there were differences in the vegetation types, coverage rates, and fertilizations [67,68], the average SOM content of the 0–30 cm depth horizon was highest in the woodland, followed by the cultivated land and the sparse forest grassland, and it was the lowest in the grassland, with values of 16.63, 11.36, 7.76, and 6.30 g/kg, respectively (Figure 4). This was consistent with the results of a previous study [69]. During decomposition of SOM by microorganisms, organic acids were released into the Quaternary ancient red soil, which promoted the transformation of silicate-bound iron oxides into poorly crystalline iron oxides [70]. Compared with the buried ancient red soil, the Fe_o contents of the 0–30 cm depth horizon of the exposed ancient red soils under different land use patterns were higher. It was the highest in the grassland, followed by the woodland and the cultivated land, and it was the lowest in the sparse forest grassland, with values of 1.77, 1.58, 1.48, and 1.33 g/kg, respectively (Figure 4). Part of the newly formed Fe_o in the topsoil was leached downward through absorption onto clay particles or in combination with SOM, and then deposited in the subsoil [71]. This is evidenced by the limited presence of Fe–Mn nodules in the subsoil (Table 2). Another part of the newly formed Fe_o was transformed into Fed-Feo [72,73]. However, SOM could reduce the oxidation rate of the iron oxides by coprecipitating with or absorbing onto the surface of reactive iron oxides [74,75], which inhibited the transformation of Fe_o to Fed-Feo [76,77]. In this study, significant negative correlations were found between the SOM content and the Fed-Feo content and (Fed-Feo)/Fed ratio (Figure 7). This is consistent with the results of a previous study, i.e., SOM decreased the degree of iron crystallinity [78]. As a result, compared with the buried ancient red soil, the average Fed-Feo contents of the 0–30 cm depth horizon in the woodland and the cultivated land decreased to 10.77 and 12.10 g/kg, respectively, due to relatively high SOM contents, while that in the grassland remained basically unchanged due to a relatively low SOM content. By contrast, due to dust fixation, the contents of iron oxides in different forms increased [79]. The average Fed-Feo content of the 0–30 cm depth horizon in the sparse forest grassland increased to 14.02 g/kg (Figure 4).

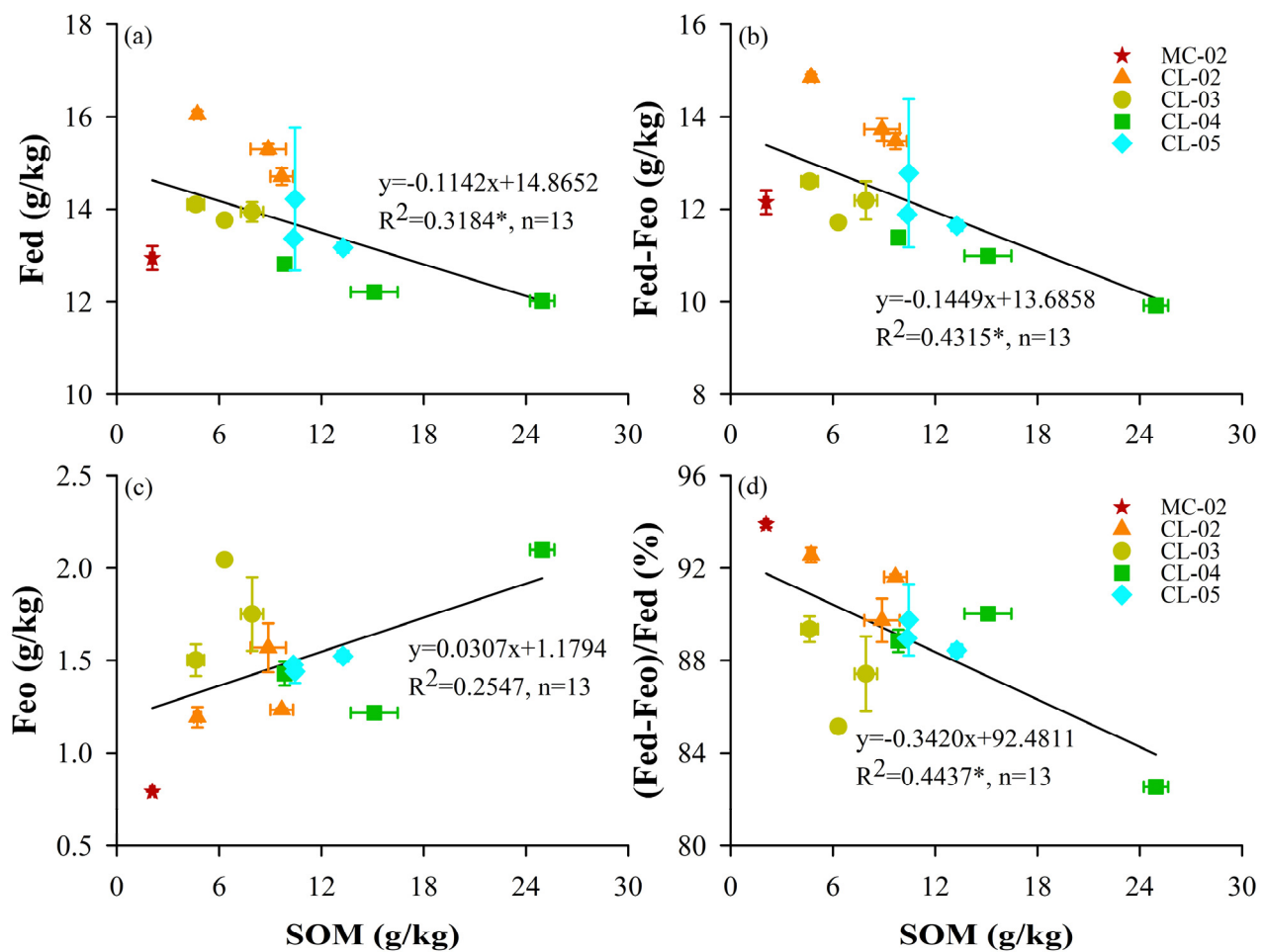


Figure 7. Correlation analysis of the relationships between the (a) Fed, (b) Fed-Feo, (c) Feo, and (d) (Fed-Feo)/Fed ratio and the SOM of the Quaternary ancient red soils under different land use patterns. Note: “*” indicates that significant differences exist in the relationships between the form of iron oxide and the iron crystalline index and the soil organic matter ($p < 0.05$).

4.2. Soil Dominant Aggregate Binding Agent Dynamics of the Quaternary Ancient Red Soils under Different Land Use Patterns

Through RDA between the aggregate compositions and aggregate binding agents of the investigated red soils, SOM and Fed were found to be the dominant binding agents in aggregate formation, with relative contribution rates of 72.00% and 26.40%, respectively (Figure 5a,d). Similar results have been reported for red soils under long-term fertilization [80]. However, TCL did not play a significant role. This is not consistent with the results of a previous study, i.e., TCL and SOM were the dominant aggregate binding agents in gray cinnamomic soil [34]. The possible reason is that the dominant aggregates bound by TCL have poor stability [30] and easily break down under changes in the ion type in the soil solution [81]. They were easily dispersed or broken by Na^+ from the loess sediments in the Quaternary ancient red soils where the deposition was synchronous with pedogenesis. Therefore, TCL may act more as bound materials rather than as a binding agent in the aggregate formation of Quaternary ancient red soils.

Furthermore, the aggregate composition of the Quaternary ancient red soil changed greatly after utilization (Figure 3), indicating the aggregate binding process changed. Before 91.01 ka BP, the red soil was buried under loess and mainly composed of <0.25 mm microaggregates, accounting for 71.62%. The aggregate formation was attributed to binding agent dynamics, such as the formation and decomposition of organic matter or the activation and crystallization of iron oxides [27,35,36]. However, in fact, aggregates of the buried

ancient red soil maintained its original state and binding agents likely remained unchanged due to compaction. Hence, there was no dominant aggregate binding agent in the buried ancient red soil (Figure 5b,e). From 91.01 ka to the present, the red soil was exposed at the surface through denudation and then affected by human activities. Compared with the buried ancient red soils, the exposed red soils under different land use patterns experienced the importation of soil organic matter, weathering of silicate-bound iron oxides, and crystallization of poorly crystalline iron oxides. Under the influence of binding agent dynamics, the <0.25 mm microaggregates were bound together into >0.25 mm macroaggregates [5,22,82,83], as evidenced by the increases in the >5, 2–5, 1–2, and 0.5–1 mm aggregate content and the decreases in the 0.053–0.25 and <0.053 mm aggregate contents (Figure 3). This is consistent with conclusions of a previous study [84]. With the new aggregate formation, the dominant aggregate binding agents changed into SOM and Fed (Figure 5c,f). Generally, aggregate formation is attributed to organic matter in soils with a relatively high content of organic binding agents and a low content of inorganic binding agents [35,36]. It is also attributed to iron oxides in soils with a relatively high content of inorganic binding agents and a low content of organic binding agents [27]. Compared with the buried ancient red soil, the average SOM contents of the woodland and the cultivated land were higher due to vegetation return and fertilization [68,85], with values of 16.63 and 11.36 g/kg, respectively. This strongly inhibited the crystallization of Feo and decreased their average Fed-Feo contents to 10.77 and 12.10 g/kg, respectively. Additionally, aggregate formation was dominated by SOM (Figure 6c,d), accounting for 95.50% and 86.10%, respectively (Figure 6g,h). This is consistent with a previous study [86]. The average SOM content of the grassland only increased to 6.30 g/kg due to difficulties in decomposing horsetails by microorganisms [65]. The average Fed-Feo content remained unchanged due to the low SOM content. The organic and inorganic binding agents were all relatively low in concentration in the grassland. SOM and Fed-Feo were not the dominant aggregate binding agents (Figure 6b,f). By contrast, the average Fed-Feo content of the sparse forest grassland increased to 14.02 g/kg due to dust fixation [79]. Further, the SOM content only increased to 7.76 g/kg due to low coverage rates and limited decomposition of vegetation by microorganisms. Its inorganic binding agents were relatively high in concentration, indicating the dominant binding agent as Fed-Feo with a relative contribution of 74.20% (Figure 6a,e).

The proportions of organic and inorganic binding agents were different and, thus, the dominant binding agents involved in aggregate formation were different. Therefore, we ask the following question: What were the proportions of organic and inorganic binding agents in the Quaternary ancient red soil when they played a dominant role in aggregate formation? To systematically answer this question, the C/Fe molar ratio was used to reflect the states of the organic matter and iron oxides during aggregate formation [87]. Based on the above analysis of the importance of Fed-Feo in the aggregate formation of Quaternary ancient red soils, correlation analysis between the relative contribution rate of the binding agents and the C/(Fed-Feo) molar ratio was carried out to obtain this threshold (Figure 8). The C/(Fed-Feo) molar ratio was significantly correlated with the relative contribution rates of SOM and Fed-Feo. When the C/(Fed-Feo) molar ratio was less than 2.13, aggregate formation was mainly attributed to the activation and crystallization of iron oxides. When the C/(Fed-Feo) molar ratio was greater than 2.13, aggregate formation was mainly attributed to the formation and decomposition of organic matter, and the crystallization of Feo was strongly inhibited (Figures 8 and 9).

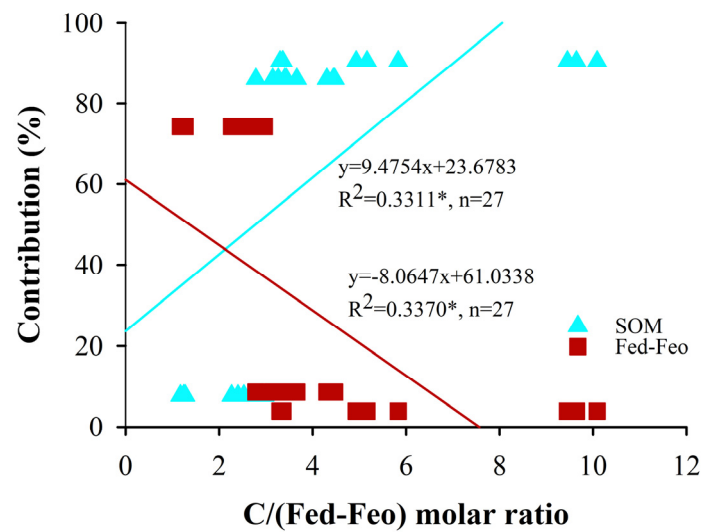


Figure 8. Correlation analysis of the relationship between the relative contribution rate and C/(Fed-Feo) molar ratio of the Quaternary ancient red soils under different land use patterns. Note: “*” indicates that significant differences exist in the relationship between the C/(Fed-Feo) ratio and the relative contribution rate ($p < 0.05$).

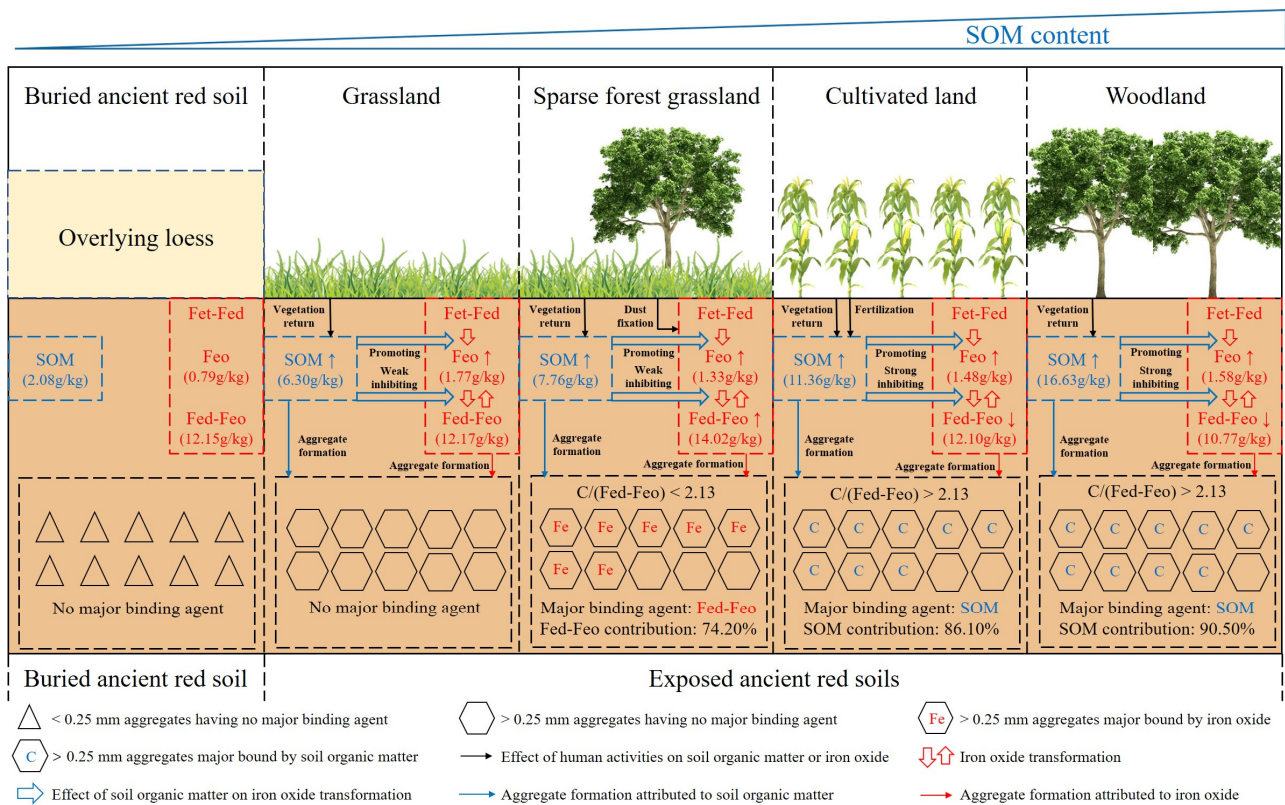


Figure 9. Conceptual model of the dominant aggregate binding agent dynamics of the Quaternary ancient red soils under different land use patterns.

5. Conclusions

The evolution sequence of investigated Quaternary ancient red soils had uniformity in parent materials. Before 91.01 ka BP, the buried ancient red soil was mainly composed of <0.25 mm aggregates and had no dominant binding agents in aggregate formation. From 91.01 ka BP to the present, the Quaternary ancient red soil was exposed at the surface through denudation and then affected by land use patterns. Compared with the buried

ancient red soils, the contents of SOM and Feo of exposed ancient red soils under different land use patterns increased. The Fed contents of the sparse forest grassland, grassland, and cultivated land increased, while those of the woodland decreased. The Fed-Feo contents in the sparse forest grassland and grassland increased, while those of the woodland and the cultivated land decreased. Under the influence of binding agent dynamics, the <0.25 mm microaggregates were bound together into >0.25 mm macroaggregates, causing the dominant aggregate binding agents in the aggregate formation of the exposed Quaternary ancient red soils to change to SOM and Fed. When the C/(Fed-Feo) molar ratio was less than 2.13, Fed-Feo was the dominant aggregate binding agent. When the C/(Fed-Feo) molar ratio was greater than 2.13, SOM was the dominant aggregate binding agent.

Author Contributions: Conceptualization, Z.S., Q.W. and G.Z.; methodology, Z.S., S.D., Y.J., Q.W. and G.Z.; software, Z.S., S.D. and Y.J.; validation, Z.S., Q.W. and G.Z.; formal analysis, Z.S., S.D. and Y.J.; investigation, Z.S., S.D., Y.J. and Q.W.; resources, Z.S., Q.W. and G.Z.; data curation, Z.S., S.D. and Y.J.; writing—original draft preparation, Z.S., S.D. and Y.J.; writing—review and editing, Z.S., Q.W. and G.Z.; visualization, Z.S., Q.W. and G.Z.; supervision, Z.S., Q.W. and G.Z.; project administration, Z.S. and Q.W.; funding acquisition, Z.S. and Q.W. All authors have read and agreed to the published version of the manuscript.

Funding: This research was funded by grants from the Postdoctoral Research Foundation of China (No. 2018M640531), the National Natural Science Foundation of China (No. 42277285, No. 41807002, and No. 41771245), the Special Foundation for National Science and Technology Basic Research Program of China (2021FY100405), the Scientific Research Fund of Liaoning Provincial Education Department (LSNQN202007), and the Department of Science and Technology of Liaoning Province (Liaoning Province Doctoral Startup Fund: No. 20170520407).

Data Availability Statement: All data are true, valid and can be available.

Acknowledgments: The authors sincerely thank all the staff and students who provided input to this study. Our acknowledgements also extend to the anonymous reviewers for their constructive reviews of the manuscript.

Conflicts of Interest: The authors declare no conflict of interest. The funders had no role in the design of the study; in the collection, analyses, or interpretation of data; in the writing of the manuscript; or in the decision to publish the results.

References

1. Edwards, A.P.; Bremner, J.M. Microaggregates in Soils. *Eur. J. Soil Sci.* **1967**, *18*, 64–73. [[CrossRef](#)]
2. Kemper, W.D.; Rosenau, R.C. Aggregate Stability and Size Distribution. *Methods Soil Anal.* **1986**, *9*, 425–442.
3. Xu, J.B.; Li, C.L.; He, Y.Q.; Wang, Y.L.; Liu, X.L. Effect of Fertilization on Organic Carbon Content and Fractionation of Aggregates in Upland Red Soil. *Acta Pedol. Sin.* **2007**, *44*, 675–682.
4. Chen, E.F.; Zhou, L.K.; Wu, G.Y. Performances of Soil Microaggregates in Storing and Supplying Moisture and Nutrients and Role of their Compositional Proportion in Judging Fertility Level. *Acta Pedol. Sin.* **1994**, *31*, 18–25.
5. Tisdall, J.M.; Oades, J.M. Organic Matter and Water-stable Aggregates in Soils. *Soil Sci.* **1982**, *33*, 141–163. [[CrossRef](#)]
6. Wu, J. *Effect of Different Tillage Measures on Soil Aggregate Stability of Dry Farmland of the Loess Plateau*; Gansu Agricultural University Press: Lanzhou, China, 2015.
7. Stevenson, F.J. *Geochemistry of Soil Humic Substances*; John Wiley and Sons Press: New York, NY, USA, 1985.
8. Wershaw, R.L.; Llaguno, E.C.; Leenheer, J.A. Mechanism of Formation of Humus Coatings on Mineral Surfaces 3. Composition of Adsorbed Organic Acids from Compost Leachate on Alumina by Solid-state ¹³C NMR. *Colloids and Surfaces A. Physicochem. Eng. Asp.* **1996**, *108*, 213–223. [[CrossRef](#)]
9. Kay, B.D. *Soil Structure and Organic Carbon: A Review*; CRC Press: Boca Raton, FL, USA, 1998.
10. Haynes, R.J.; Beare, M.H. Influence of Six Crop Species on Aggregate Stability and Some Labile Organic Matter Fractions. *Soil Biol. Biochem.* **1997**, *29*, 1647–1653. [[CrossRef](#)]
11. Martens, D.A. Plant Residue Biochemistry Regulates Soil Carbon Cycling and Carbon Sequestration. *Soil Biol. Biochem.* **2000**, *32*, 361–369. [[CrossRef](#)]
12. Bronick, C.J.; Lal, R. Soil Structure and Management: A Review. *Geoderma* **2005**, *124*, 3–22. [[CrossRef](#)]
13. Magill, A.H.; Aber, J.D. Long-term Effects of Experimental Nitrogen Additions on Foliar Litter Decay and Humus Formation in Forest Ecosystems. *Plant Soil* **1998**, *203*, 301–311. [[CrossRef](#)]
14. Caesar-Tonthat, T.C. Soil Binding Properties of Mucilage Produced by A Basidiomycete Fungus in A Model System. *Mycol. Res.* **2002**, *106*, 930–937. [[CrossRef](#)]

15. Diné, H.; Righi, D.; Hardy, M.; Jambu, P. Neutral Lipids and Structural Stability of Physically Degraded Soils. *Agrochimica* **1997**, *41*, 97–108.
16. Pare, T.; Diné, H.; Moulin, A.P.; Townley-Smith, L. Organic Matter Quality and Structural Stability of A Black Chernozemic Soil under Different Manure and Tillage Practices. *Geoderma* **1999**, *91*, 311–326. [[CrossRef](#)]
17. Fedoroff, N. Clay illuviation in Red Mediterranean soils. *Catena* **1997**, *28*, 171–184. [[CrossRef](#)]
18. Yaalon, D.H. Soils in the Mediterranean region: What makes them different? *Catena* **1997**, *28*, 157–169. [[CrossRef](#)]
19. Durn, G. Terra Rossa in the Mediterranean Region: Parent materials, composition and origin. *Geol. Croat.* **2003**, *56*, 83–100. [[CrossRef](#)]
20. Fedoroff, N.; Courty, M.A. Revisiting the genesis of red Mediterranean soil. *Turk. J. Earth Sci.* **2013**, *22*, 359–375. [[CrossRef](#)]
21. Wang, L.Y.; Qin, L.; Lv, X.G.; Jiang, M.; Zou, Y.C. Progress in Researches on Effect of Iron Promoting Accumulation of Soil Organic Carbon. *Acta Pedol. Sin.* **2018**, *55*, 4–13.
22. Oades, J.M.; Gillman, G.P.; Uehara, G. *Interactions of Soil Organic Matter and Variable Charge Clays*; University of Hawaii Press: Manoa Valley, HI, USA, 1989.
23. El-Swaify, S.A.; Emerson, W.W. Changes in the Physical Properties of Soil Clays Due to Precipitated Aluminum and Iron Hydroxides: I. Swelling and Aggregate Stability after Drying. *Soil Sci. Soc. Am. J.* **1975**, *39*, 1056–1063. [[CrossRef](#)]
24. Muggler, C.C.; Griethuysen, B.P.; Pape, T. Aggregation, Organic Matter, and Iron Oxide Morphology in Oxisols from Minas Gerais, Brazil. *Soil Sci.* **1999**, *164*, 759–770. [[CrossRef](#)]
25. Shang, L.L. *The Effect of Long-Term Fertilization and Land Use Pattern on Red Soil Aggregate Stability*; Huazhong Agricultural University: Wuhan, China, 2014.
26. Hou, T.; Xu, R.K.; Tiwari, D.; Zhao, A.Z. Interaction between Electric Double Layers of Kaolinite and Fe/Al Oxides in Suspensions. *J. Colloid Interface Sci.* **2007**, *310*, 670–674. [[CrossRef](#)] [[PubMed](#)]
27. Yu, X.L. *Three-Dimensional Structures, Forming Process and Environmental Significance of Soil Aggregate and Fe-Mn Nodules*; Zhejiang University Press: Hangzhou, China, 2015.
28. Bai, X.M.; Han, Y.Z.; Guo, H.Q. Characteristics of Soil Macroaggregates under Typical Forests in Pangquangou Nature Reserve. *Acta Ecol. Sin.* **2014**, *34*, 1654–1662.
29. Wang, T.; He, B.H.; Qin, C.; Li, T.Y. The Composition and Stability of Soil Aggregates with Different Planting Years of *Hemerocallis Citrina* in Terrace Biological Bank. *J. Soil Water Conserv.* **2014**, *28*, 153–158.
30. Zhang, Y.F.; Zhao, S.W.; Wang, Z.L.; Li, X.X.; Li, M.R.; Du, C. Distribution and Function of Cementing Materials of Soil Aggregates on the Loess Plateau, Western China. *Sci. Soil Water Conserv.* **2015**, *13*, 145–150.
31. Sakurai, K.; Teshima, A.; Kyuma, K. Changes in Zero Point of Charge (ZPC), Specific Surface Area (SSA), and Cation Exchange Capacity (CEC) of Kaolinite and Montmorillonite, and Strongly Weathered Soils Caused by Fe and Al Coatings. *Soil Sci. Plant Nutr.* **1990**, *36*, 73–81. [[CrossRef](#)]
32. Amézketa, E. Soil Aggregate Stability: A Review. *J. Sustain. Agric.* **1999**, *14*, 83–151. [[CrossRef](#)]
33. Chen, Y.Y.; Zhao, W.J.; Jia, Y.G.; Xu, G.C. The Influence of Clay and Organic Matter on the Sediment Aggregation in the Yellow River Estuary. *Mar. Geol. Quat. Geol.* **2009**, *29*, 31–37. [[CrossRef](#)]
34. An, S.S.; Huang, Y.M.; Li, B.C.; Yang, J.G. Characteristics of Soil Water Stable Aggregates and Relationship with Soil Properties during Vegetation Rehabilitation in A Loess Hilly Region. *Chin. J. Soil Sci.* **2006**, *37*, 45–50.
35. Zhang, B.; Horn, R. Mechanisms of Aggregate Stabilization in Ultisols from Subtropical China. *Geoderma* **2001**, *99*, 123–145. [[CrossRef](#)]
36. Cui, X.Y.; Gao, F.; Song, J.F.; Sang, Y.; Sun, J.B.; Di, X.Y. Changes in Soil Total Organic Carbon after An Experimental Fire in A Cold Temperate Coniferous Forest: A Sequenced Monitoring Approach. *Geoderma* **2014**, *226–227*, 260–269. [[CrossRef](#)]
37. Arduino, E.; Barberis, E.; Boero, V. Iron Oxides and Particle Aggregation in B horizons of Some Italian Soils. *Geoderma* **1989**, *45*, 319–329. [[CrossRef](#)]
38. Han, C.L.; Liu, S.H.; Wang, Q.B.; Wang, H.Q. Basic Properties and Genetic Characteristic Research of Quaternary Paleosol in Chaoyang City of Liaoning. *Chin. J. Soil Sci.* **2009**, *40*, 1233–1239.
39. Duan, S.Y.; Sun, Z.X.; Wang, Q.B.; Jiang, Y.Y.; Han, C.L.; Zhang, Y.W.; Lv, M.F.; Sun, F.J.; Chen, L.M. Characteristics of Soil Organic Carbon Distribution of Quaternary Red Soils under Different Land Use Patterns. *Chin. J. Soil Sci.* **2021**, *52*, 1078–1084.
40. Duan, S.Y.; Sun, Z.X.; Wang, Q.B.; Jiang, Y.Y.; Sun, F.J. Comparison of Aggregate Composition in Quaternary Red Soils under Different Land Use Patterns. *Chin. J. Soil Sci.* **2020**, *51*, 587–596.
41. Jia, W.J. *Soils of Liaoning*; Liaoning Science and Technology Press: Shenyang, China, 1992.
42. Wang, Q.B.; Han, C.L.; Sun, F.J.; Sun, Z.X. *Soil Series of China Liaoning*; Science Press: Beijing, China, 2020.
43. Chinese Soil Taxonomy Research Group; Institute of Soil Science Chinese Academy of Sciences; Cooperative Research Group on Chinese Soil Taxonomy. *Keys to Chinese Soil Taxonomy*, 3rd ed.; University of Science and Technology of China Press: Hefei, China, 2001. (In Chinese)
44. Soil Survey Staff. *Keys to Soil Taxonomy*, 12th ed.; U.S. Natural Resources Conservation Service Government Printing Office: Washington, DC, USA, 2014.
45. IUSS Working Group WRB. *World Reference Base for Soil Resources 2014, Update 2015 International Soil Classification System for Naming Soils and Creating Legends for Soil Maps*; World Soil Resources Reports No. 106; FAO: Rome, Italy, 2015.
46. Zhang, G.L.; Gong, Z.T. *Manual of Soil Description and Sampling*; Science Press: Beijing, China, 2012.

47. Bronger, A.; Catt, J.A. Paleosols: Problems of Definition, Recognition and Interpretation. *Catena* **1989**, *16*, 1–7.
48. Grossman, R.B.; Reinsch, T.G. Bulk Density and Linear Extensibility. In *Methods of Soil Analysis: Part 4 Physical Methods*; Dane, J.H., Topp, G.C., Eds.; ASA and SSSA: Madison, WI, USA, 2002; pp. 201–228.
49. Wintle, A.G. Luminescence dating: Laboratory procedures and protocols. *Radiat. Measur.* **1997**, *27*, 769–817. [[CrossRef](#)]
50. Murray, A.S.; Wintle, A.G. Luminescence dating of quartz using an improved single-aliquot regenerative-dose protocol. *Radiat. Meas.* **2000**, *32*, 57–73. [[CrossRef](#)]
51. Domal, H.; Hodara, J.; Slowinska, J.A.; Turski, R. The Effects of Agricultural Use on the Structure and Physical Properties of Three Soil Types. *Soil Tillage Res.* **1993**, *27*, 365–382.
52. Xue, B. *The Characteristics of Cementing Material and Stability of Soil Aggregates under Straw Returning in Rice-Rape Cropping System*; Huazhong Agricultural University Press: Wuhan, China, 2020.
53. Zhang, Y.H. *Characteristics of Soil Aggregates and Organic Carbon Components in Black Soil under Different Land Use*; Northeast Agricultural University Press: Haerbin, China, 2018.
54. Yoder, R.E. A Direct Method of Aggregate Analysis of Soils and A Study of the Physical Nature of Erosion Losses. *Soil Sci. Soc. Am. J.* **1936**, *28*, 337–351.
55. Bcare, Y.G.; Wander, M.M. Tillage Effects on Aggregate Turnover and Sequestration of Particulate and Humified Soil Organic Carbon. *Soil Sci. Soc. Am. J.* **2008**, *72*, 670–676.
56. Li, J.W.; Jiao, X.G.; Sui, Y.Y.; Cheng, S.J. The Belonging of Dark Brown Soil in the East of Jilin Province in Chinese Soil Taxonomy. *Chin. Agric. Sci. Bull.* **2011**, *27*, 74–79.
57. Mehra, O.P.; Jackson, M.L. Iron oxide removal from soils and clays by a dithionite–citrate system buffered with sodium bicarbonate. *Clays Clay Miner.* **1958**, *7*, 317–327. [[CrossRef](#)]
58. McKeague, J.A.; Day, J.H. Dithionite and Oxalate Extractable Fe and Al as Aids in Differentiating Various Classes of Soils. *Can. J. Soil Sci.* **1966**, *46*, 13–22. [[CrossRef](#)]
59. Lu, H.Y.; An, Z.S. An experimental study on the effect of pretreatment methods for the particle size determination of loess sediment. *Chin. Sci. Bull.* **1997**, *42*, 2535–2538.
60. Schaetzl, R.J. Lithologic Discontinuities in Some Soils on Drumlins: Theory, Detection, and Application. *Soil Sci.* **1998**, *163*, 570–590. [[CrossRef](#)]
61. Tsai, C.C.; Chen, Z.S. Lithologic Discontinuities in Ultisols along A Toposequence in Taiwan. *Soil Sci.* **2000**, *165*, 587–596. [[CrossRef](#)]
62. Essington, M.E. *Soil and Water Chemistry: An Integrative Approach*; CRC Press: Boca Raton, FL, USA, 2003.
63. Sun, Z.X.; Wang, Q.B.; Han, C.L.; Zhang, Q.J.; Owens, P.R. Clay mineralogical characteristics and the palaeoclimatic significance of a Holocene to Late Middle Pleistocene loess-palaeosol sequence from Chaoyang, China. *Earth Environ. Sci. Trans. R. Soc. Edinburgh.* **2016**, *106*, 185–197. [[CrossRef](#)]
64. Sun, Z.X.; Jiang, Y.Y.; Wang, Q.B.; Jiang, Z.D.; Libohova, Z.; Owens, P.R. Characteristics of a Benchmark Loess–Paleosol Profile in Northeast China. *Agronomy* **2022**, *12*, 1376. [[CrossRef](#)]
65. Brewer, R. Fabric and Mineral Analysis of Soils. *Soil Sci.* **1965**, *100*, 73. [[CrossRef](#)]
66. Schaetzl, R.J.; Anderson, S. *Soils: Genesis and Geomorphology*; Cambridge University Press: New York, NY, USA, 2005.
67. Palm, C.A.; Gachengo, C.N.; Delve, R.J.; Cadisch, G.; Giller, K.E. Organic Inputs for Soil Fertility Management in Tropical Agroecosystems: Application of An Organic Resource Database. *Agric. Ecosyst. Environ.* **2001**, *83*, 27–42. [[CrossRef](#)]
68. Ledo, A.; Smith, P.; Zerhun, A.; Whitaker, J.; Vicente-Vicente, J.L.; Qin, Z.C.; Mcnamara, N.P.; Zinn, Y.L.; Llorente, M.; Liebig, M.; et al. Changes in Soil Organic Carbon under Perennial Crops. *Glob. Chang. Biol.* **2020**, *26*, 4158–4168. [[CrossRef](#)]
69. Midwood, A.J.; Hannam, K.D.; Gebretsadikan, T.; Emde, D. Storage of Soil Carbon as Particulate and Mineral Associated Organic Matter in Irrigated Woody Perennial Crops. *Geoderma* **2021**, *403*, 115185. [[CrossRef](#)]
70. Huang, W.H.; Keller, W.D. Dissolution of Rock-forming Silicate Minerals in Organic Acids; Simulated First-stage Weathering of Fresh Mineral Surfaces. *Am. Mineral.* **1970**, *55*, 2076–2094.
71. Li, T.J.; Zhao, Y.; Zhang, K.L. *Soil Geography*; Higher Education Press: Beijing, China, 2004.
72. Alexander, E.B. Estimating Relative Ages from Iron-oxide/total-iron Ratios of Soils in the Western Po Valley, Italy—A Discussion. *Geoderma* **1985**, *35*, 257–258. [[CrossRef](#)]
73. Aniku, J.; Singer, M.J. Pedogenic Iron Oxide Trends in A Marine Terrace Chronosequence. *Soil Sci. Soc. Am. J.* **1990**, *54*, 147–152. [[CrossRef](#)]
74. Chen, C.; Kukkadapu, R.; Sparks, D.L. Influence of Coprecipitated Organic Matter on Fe²⁺ (aq)-catalyzed Transformation of Ferrihydrite: Implications for Carbon Dynamics. *Environ. Sci. Technol.* **2015**, *49*, 10927–10936. [[CrossRef](#)]
75. Thomas, A.L.K.; Mikutta, C.; Byrne, J.; Kappler, A.; Kretzschmar, R. Iron (II)-Catalyzed Iron Atom Exchange and Mineralogical Changes in Iron-rich Organic Freshwater Floccs: An Iron Isotope Tracer Study. *Environ. Sci. Technol.* **2017**, *51*, 6897–6907.
76. Schwertmann, U. Inhibitory Effect of Soil Organic Matter on the Crystallization of Amorphous Ferric Hydroxide. *Nature* **1966**, *212*, 645–646. [[CrossRef](#)]
77. Sun, L.R. *Study on Dissimilatory Reduction of Iron Oxides in Paddies and Its Influential Factors*; Northwest A & F University Press: Xianyang, China, 2007.
78. Chen, C.M.; Thompson, A. Ferrous Iron Oxidation under Varying pO₂ Levels: The Effect of Fe (III)/Al (III) Oxide Minerals and Organic Matter. *Environ. Sci. Technol.* **2018**, *52*, 597–606. [[CrossRef](#)]

79. Sun, Z.X.; Jiang, Y.Y.; Wang, Q.B.; Sun, F.J.; Zhang, M.G. A Comparative Analysis between Local Soils and Dust Deposition on Snow in Shenyang, China and Implications on Loess-paleosols Evolution. *Geoderma* **2019**, *342*, 34–41. [[CrossRef](#)]
80. Yan, X. *Effects of Long-Term Fertilization on Soil Fertility, Organic Carbon Pools and Soil Aggregation in Paddy Soil and Upland Red Soil*; Hunan Agricultural University Press: Changsha, China, 2013.
81. Huang, C.Y. *Soil Science*; China Agriculture Press: Beijing, China, 1999.
82. Oades, J.M. Soil Organic Matter and Structural Stability: Mechanisms and Implications for Management. *Plant Soil*. **1984**, *76*, 319–337. [[CrossRef](#)]
83. Six, J.; Elliott, E.T.; Paustian, K. Soil Macroaggregate Turnover and Microaggregate Formation: A Mechanism for C Sequestration under No-tillage Agriculture. *Soil Biol. Biochem.* **2000**, *32*, 2099–2103. [[CrossRef](#)]
84. Zhao, J.S.; Chen, S.; Hu, R.G.; Li, Y.Y. Aggregate stability and size distribution of red soils under different land uses integrally regulated by soil organic matter, and iron and aluminum oxides. *Soil Tillage Res.* **2017**, *167*, 73–79. [[CrossRef](#)]
85. Golchin, A.; Clarke, P.; Oades, J.M.; Skjemstad, J.O. The Effects of Cultivation on the Composition of Organic-matter and Structural Stability of Soils. *Aust. J. Soil Res.* **1995**, *33*, 16–25. [[CrossRef](#)]
86. Zhang, Z.B.; Zhou, H.; Lin, H.; Peng, X. Puddling Intensity, Sesquioxides, and Soil Organic Carbon Impacts on Crack Patterns of Two Paddy Soils. *Geoderma* **2016**, *262*, 155–164. [[CrossRef](#)]
87. Coward, E.K.; Ohno, T.; Plante, A.F. Adsorption and Molecular Fractionation of Dissolved Organic Matter on Iron-bearing Mineral Matrices of Varying Crystallinity. *Environ. Sci. Technol.* **2018**, *52*, 1036–1044. [[CrossRef](#)]

Disclaimer/Publisher’s Note: The statements, opinions and data contained in all publications are solely those of the individual author(s) and contributor(s) and not of MDPI and/or the editor(s). MDPI and/or the editor(s) disclaim responsibility for any injury to people or property resulting from any ideas, methods, instructions or products referred to in the content.